

# Northumbria Research Link

Citation: Shelyag, Sergiy (2015) Spectro-polarimetric simulations of the solar limb: absorption-emission Fe I 6301.5 Å AND 6302.5 Å line profiles and torsional flows in the intergranular magnetic flux concentrations. The Astrophysical Journal, 801 (1). p. 46. ISSN 1538-4357

Published by: The American Astronomical Society

URL: <http://dx.doi.org/10.1088/0004-637X/801/1/46> <<http://dx.doi.org/10.1088/0004-637X/801/1/46>>

This version was downloaded from Northumbria Research Link:  
<http://nrl.northumbria.ac.uk/id/eprint/26891/>

Northumbria University has developed Northumbria Research Link (NRL) to enable users to access the University's research output. Copyright © and moral rights for items on NRL are retained by the individual author(s) and/or other copyright owners. Single copies of full items can be reproduced, displayed or performed, and given to third parties in any format or medium for personal research or study, educational, or not-for-profit purposes without prior permission or charge, provided the authors, title and full bibliographic details are given, as well as a hyperlink and/or URL to the original metadata page. The content must not be changed in any way. Full items must not be sold commercially in any format or medium without formal permission of the copyright holder. The full policy is available online: <http://nrl.northumbria.ac.uk/policies.html>

This document may differ from the final, published version of the research and has been made available online in accordance with publisher policies. To read and/or cite from the published version of the research, please visit the publisher's website (a subscription may be required.)

# SPECTRO-POLARIMETRIC SIMULATIONS OF THE SOLAR LIMB: ABSORPTION-EMISSION Fe I 6301.5Å AND 6302.5Å LINE PROFILES AND TORSIONAL FLOWS IN THE INTERGRANULAR MAGNETIC FLUX CONCENTRATIONS

S. SHEL'YAG

School of Mathematical Sciences, Monash University, Victoria 3800, Australia

(Dated: 01.01.01/01.01.01)  
 Draft version January 6, 2015

## ABSTRACT

Using radiative magneto-hydrodynamic simulations of the magnetised solar photosphere and detailed spectro-polarimetric diagnostics with the Fe I 6301.5Å and 6302.5Å photospheric lines in the local thermodynamic equilibrium approximation, we model active solar granulation as if it was observed at the solar limb. We analyse general properties of the radiation across the solar limb, such as the continuum and the line core limb darkening and the granulation contrast. We demonstrate the presence of profiles with both emission and absorption features at the simulated solar limb, and pure emission profiles above the limb. These profiles are associated with the regions of strong linear polarisation of the emergent radiation, indicating the influence of the intergranular magnetic fields on the line formation. We analyse physical origins of the emission wings in the Stokes profiles at the limb, and demonstrate that these features are produced by localised heating and torsional motions in the intergranular magnetic flux concentrations.

*Subject headings:* Sun: Photosphere — Sun: Surface magnetism — Plasmas — Magnetohydrodynamics (MHD)

## 1. INTRODUCTION

The solar photosphere at the limb remains one of the largely unexplored solar regions due to the lack of bright and extended emissive features, such as spicules in the chromosphere, and sharp limb darkening, associated with low light conditions and high instrumental noise levels in the observations of this region. On the other hand, the solar limb has potential for the diagnostics of parallel to the solar surface photospheric flows and magnetic fields. Together with solar disk observations, it can provide new and more detailed information on the geometry of the flow and magnetic field structures in the solar photosphere, on the details of transition between the photosphere and the chromosphere, as well as on the origins of chromospheric features.

Groundbreaking spectro-polarimetric observation of the solar limb with Hinode SOT (Tsuneta et al. 2008) by Lites et al. (2010) revealed a thin, sub-arcsecond layer of photospheric emission in the 6301.5Å and 6302.5Å lines of neutral iron. These lines, normally in absorption within the solar disk, undergo a transition into pure emission above the limb. The transition between absorption and emission is characterised by the appearance of emissive wings in the line profiles, their significant Doppler shifts, and linear (radially directed) light polarisation.

Realistic numerical simulations of solar surface magneto-convection have long been successful in reproducing, explaining and even predicting various solar photospheric (see e.g. Stein 2012, and references therein), and, recently, chromospheric phenomena (Leenaarts et al. 2012; Pereira et al. 2013). Centre-to-limb variation of solar radiation has been extensively studied using simulations (Keller et al. 2004; Koesterke et al. 2008; Kitiashvili et al. 2014). Ultimately, the success of numerical modelling in under-

standing the physics of the solar photosphere can be demonstrated by an excellent agreement between the various numerical codes used to simulate the solar surface layers (Beeck et al. 2012).

In this paper, we use numerical simulation of the solar photosphere with the MURaM code (Vögler et al. 2005) and one-dimensional line profile synthesis with the NICOLE code (Socas-Navarro et al. 2014) to perform the modelling of the spectro-polarimetric properties of the radiation at the solar limb with the 6301.5Å and 6302.5Å Fe I lines in the LTE approximation. We show the average properties of simulated radiation, such as centre-to-limb variation of the continuum intensity and the intensity in the line core. We also show the connection between the line core intensity and the linear polarisation above the limb. At the limb, we demonstrate the presence of the transition layer between pure absorption and pure emission, spectropolarimetrically similar to the observations by Lites et al. (2010). In the transition layer, the profiles with emission wings are found. Using response functions to the temperature for the 6301.5Å line, we analyse the line formation process and provide a simple model for emission-absorption line profile formation at the solar limb. In our simulations, the emission wings in the profiles are produced by positive temperature gradients and torsional line-of-sight motions within the intergranular magnetic flux tubes. In contrast to the proposed role of non-LTE scattering (Lites et al. 2010) in formation of photospheric line profiles above the limb, we are able to reproduce the wing emission in the profiles in pure one-dimensional LTE approximation. We suggest that both non-LTE scattering and Doppler-shifted emission in the flux tubes are responsible for the complex Stokes-*I* profile shapes at the solar limb.

The paper is organised as follows. In Section 2 we describe the simulation setup we used to model the solar

limb radiation and polarization information. Section 3 is divided into subsections 3.1 and 3.2, where we describe the general properties of the simulated limb, and analyse the physical origins of emission in the line profile wings at the limb, respectively. Section 4 concludes our findings.

## 2. SIMULATION SETUP

We use a single extended photospheric MHD model snapshot from a unipolar magnetic field simulation of a plage region produced by the MURaM code (Vögler et al. 2005). The code solves radiative MHD equations on a Cartesian grid. The magneto-convection simulation is set through injecting a uniform magnetic field of 200 G into a previously calculated non-magnetic convection model. The resolution is 25 km in the horizontal directions and 10 km in the vertical direction. The simulation box has a size of  $12 \times 12 \text{ Mm}^2$  and 3.2 Mm in the horizontal and vertical directions, respectively. The average continuum formation layer is located at about 2 Mm above the bottom boundary. The bottom boundary of the domain is open for in- and outflows, and the top boundary is open for outflows, while the inflows are kept at constant temperature 6000 K in order to mimic the chromospheric layers of the Sun. The side boundaries are periodic. We use FreeEOS equation of state (Irwin 2012) to account for changes in the gas law due to partial ionization. No Hall term or ambipolar diffusion is included in the simulation.

A solar limb region is constructed by adding together 16 copies of the chosen snapshot and locally changing the geometry of the snapshots to cylindrical geometry with radius  $R_\odot = 695 \text{ Mm}$  in order to mimic the curvature of the solar surface in one dimension. The final size of the domain is about  $192 \times 10 \text{ Mm}$  in the horizontal and vertical directions, respectively, which corresponds to  $\pm 8^\circ$  inclination between the surface and the line-of-sight (LOS), or  $\mu = 0 - 0.14$ . The LOS components of the magnetic field and the plasma velocity are recalculated accordingly. After the domain is projected back to the Cartesian grid, it is resampled to a somewhat lower (25 km) vertical resolution to reduce the computational cost, and smoothed along the lines-of-sight with a boxcar function with the width of 100 km to avoid numerical instabilities due to sharp gradients between granular and intergranular solar magneto-convection features during radiative transport computations. With the optical ray length of about 5 Mm the effect of the smoothing is negligible. Using the same model snapshot to cover the solar limb allows us to study the same features under the different inclination angles as well as at the solar limb. A vertical cut through half of the constructed solar limb domain is shown in Fig. 1. As is evident from the figure, in the constructed domain both the regions of the solar disk (with optically thick, hot and dense plasma) and the solar limb (optically thin) are present. The LOS components of the magnetic field and the velocity are predominantly horizontal in this simulation. Therefore, granular upflows and magnetised downflows do not influence the radiation. However, the photospheric part of the domain is covered with horizontally expanding magnetic fields and with the radially elongated line-of-sight velocity structures of alternating sign corresponding to Alfvénic horizontal torsional motions. These motions have been recently demonstrated to exist in the inter-

granular magnetic flux concentrations in simulations and analysed by Shelyag et al. (2013); Shelyag & Przybylski (2014).

In order to calculate Stokes profiles for 6301.51 Å and 6302.49 Å Fe I absorption lines, the horizontal one-dimensional columns from the solar limb model were used as an input for spectro-polarimetric line profile synthesis code NICOLE (Socas-Navarro et al. 2000; Socas-Navarro 2011; Socas-Navarro et al. 2014). No multi-dimensional scattering or non-LTE effects were included in the computation. The excitation potentials  $V = 3.65 \text{ eV}$  and  $\log gf = -0.59$ , and  $V = 3.686 \text{ eV}$  and  $\log gf = -1.13$  were used for 6301.51 Å and 6302.49 Å Fe I lines synthesis, respectively. The full Stokes vectors for the lines were calculated within 6301.2 Å – 6301.8 Å, and 6302.2 Å – 6302.8 Å wavelength ranges with 3 mÅ resolution.

## 3. RESULTS

### 3.1. General properties

The average radiation intensity structure across the simulated limb is shown in Fig. 2. The solid curve represents the normalised continuum intensity variation. A region with sharp intensity decrease from 0.5 to nearly zero at 696.6 Mm has thickness of about 200 km. At the rest wavelength of the Fe I line core,  $\lambda = 6302.49 \text{ Å}$ , the average intensity (dashed curve) is about 0.5 of the continuum intensity at the solar disk. However, due to the increased opacity in the line core, the simulated solar limb is higher in the solar atmosphere by about 300 km and spreads over a somewhat larger height range of about 300 km. Similar behaviour is demonstrated by the minimum intensity in the line profile (shown as dash-dotted curve). It should be also noted that the averaging has been done over a single computational snapshot, which does not account for the oscillations and time dependence present in the simulations. Therefore signatures of intensity variability due to granulation are also present.

Average continuum intensities across the full solar disk were also computed. Fig. 3 shows the average 6300 Å normalised intensities calculated for the same model snapshot at different observational angles at the solar disk  $\mu = 1, \sqrt{3}/2, 0.5, 0.2, 0.1, 0.05$  using the domain inclination method (see e.g. Shelyag & Przybylski 2014, black solid line), the average intensities from the limb simulation ( $\mu = 0.14 - 0$ ; green solid line), the granulation contrast (black dashed line) and the granulation contrast from the limb simulation (green dashed line). As the plot shows, the limb darkening dependences on  $\mu$  fit exactly in the overlapping region between  $\mu = 0.05 - 0.1$ . The *rms* contrast dependence on  $\mu$  for the limb simulation shows large scatter due to significantly smaller statistics. However, the scatter is found to be close around the average contrast values for the solar disk computation.

A continuum intensity image (Fig. 4, top-left panel) shows low-contrast solar limb granulation and a corrugated solar limb surface. The limb height variability due to granulation is small, of the order of 100 – 200 km, as the (deeper) intergranular lanes are completely hidden by the granulation. Bright granular walls (faculae) are visible (Keller et al. 2004). There are no noticeable continuum intensity features above the solar limb. The 6301.5 Å line core intensity image (top-right panel in Fig. 4) and,

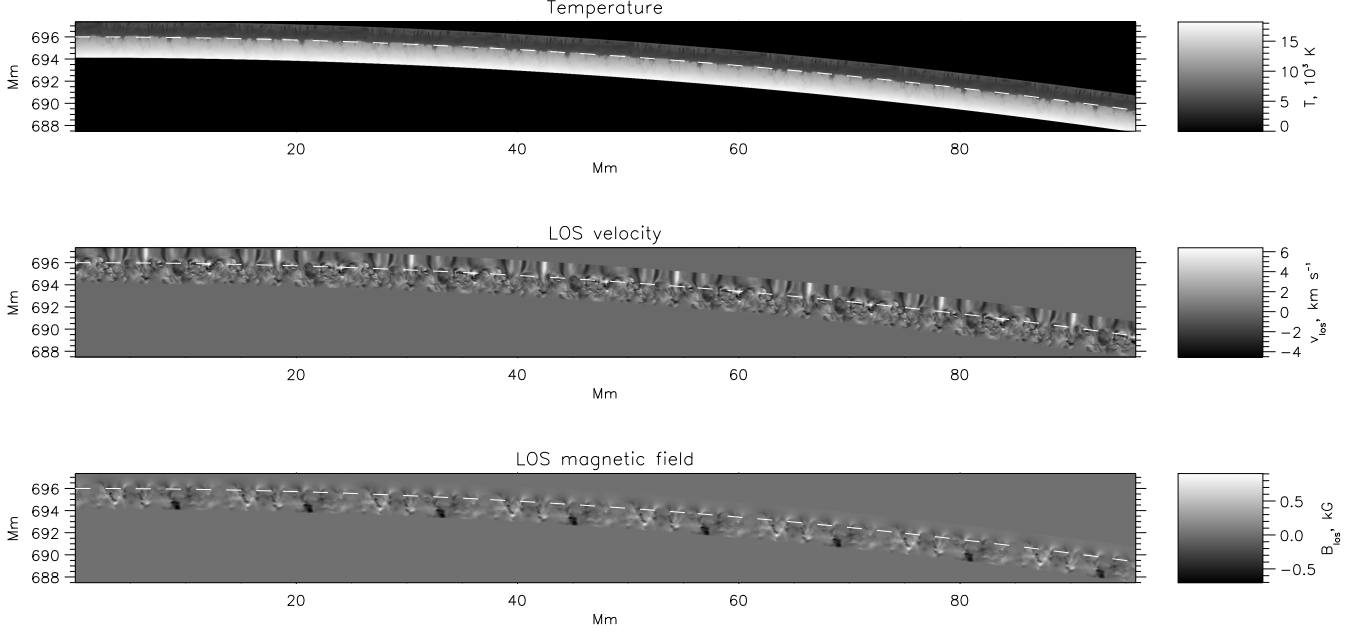


FIG. 1.— Vertical cut through a half of the simulation domain representing the solar limb. The temperature, LOS velocity and LOS magnetic field strength are shown in the upper, middle and bottom panels, respectively. The vertical axis in the plots corresponds to the distance from the solar centre. The dashed line in the panels indicates approximate level of the solar surface.

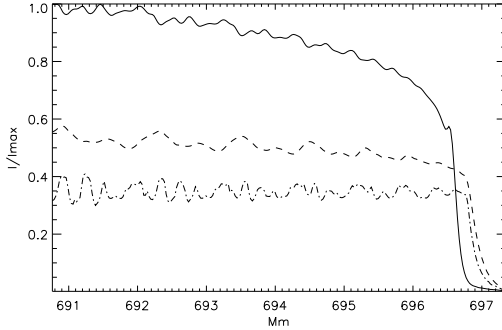


FIG. 2.— Limb darkening across the solar limb. 6300Å continuum intensity is shown with the solid line, the dashed line corresponds to the intensity at the wavelength of the line core 6302.49Å, and the dash-dotted line corresponds to the minimum intensity of the FeI 6302.49Å line profile. The horizontal axis is the distance from the solar centre.

more pronounced, the 6301.5 – 0.15Å line wing intensity image (middle-left panel), however, show a large number of small-scale vertically extending features with somewhat enhanced line core and strongly enhanced line wing intensities above the average solar limb radius at this wavelength,  $R > 697$  Mm. The 6302.5Å line core intensity (middle-right panel) shows similar, although less prominent features. Reversed granulation is also visible (Cheung et al. 2007).

As can be seen from the bottom panel of Fig. 1, the LOS magnetic field mainly corresponds to the horizontal magnetic field of the intergranular magnetic field concentrations, expanding in the solar atmosphere. Therefore, along the line of sight, both polarities of the magnetic field, as well as a strong component of the magnetic field perpendicular to the line of sight, are present. Together with torsional oscillatory flows in the magnetic

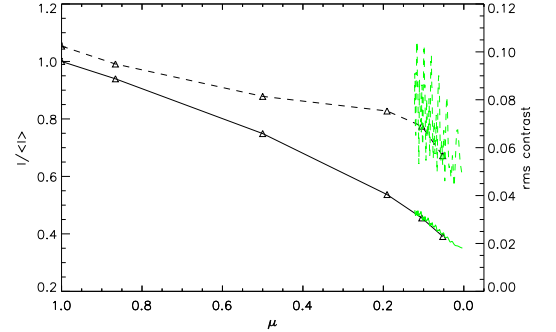


FIG. 3.— 6300Å continuum limb darkening across the solar disk. Solid curve - simulated average normalized intensity, dashed curve - rms contrast of granulation. The solar limb model ( $\mu = 0.15 - 0$ ) is shown in green. Triangles show the inclination angles used to calculate the radiation parameters,  $\mu = 1, \sqrt{3}/2, 0.5, 0.2, 0.1, 0.05$ .

flux tubes, this leads to generation of strong and asymmetric, multi-lobed profiles in all polarization components, as it is demonstrated in the next subsection.

The line parameters, namely the linear ( $\int \sqrt{Q^2 + U^2} d\lambda$ ) and circular ( $\int |V| d\lambda$ ) polarisation, are shown in the bottom-left and bottom-right panels of Fig. 4, respectively. The images show the presence of strong Stokes signals both at the solar limb and in the simulated solar disk region. As expected due to the weakness of the LOS magnetic field and strong magnetic field component perpendicular to the line-of-sight above the limb, the signal in Stokes- $V$  becomes weaker, and the signal in  $\sqrt{Q^2 + U^2}$  becomes stronger above the solar limb region.

Scatter plots of the intensity in the line core versus total Stokes- $V$  and  $\sqrt{Q^2 + U^2}$  areas are shown in the left and right panels of Fig. 5, respectively. Both figures clearly show two separate populations of points: above



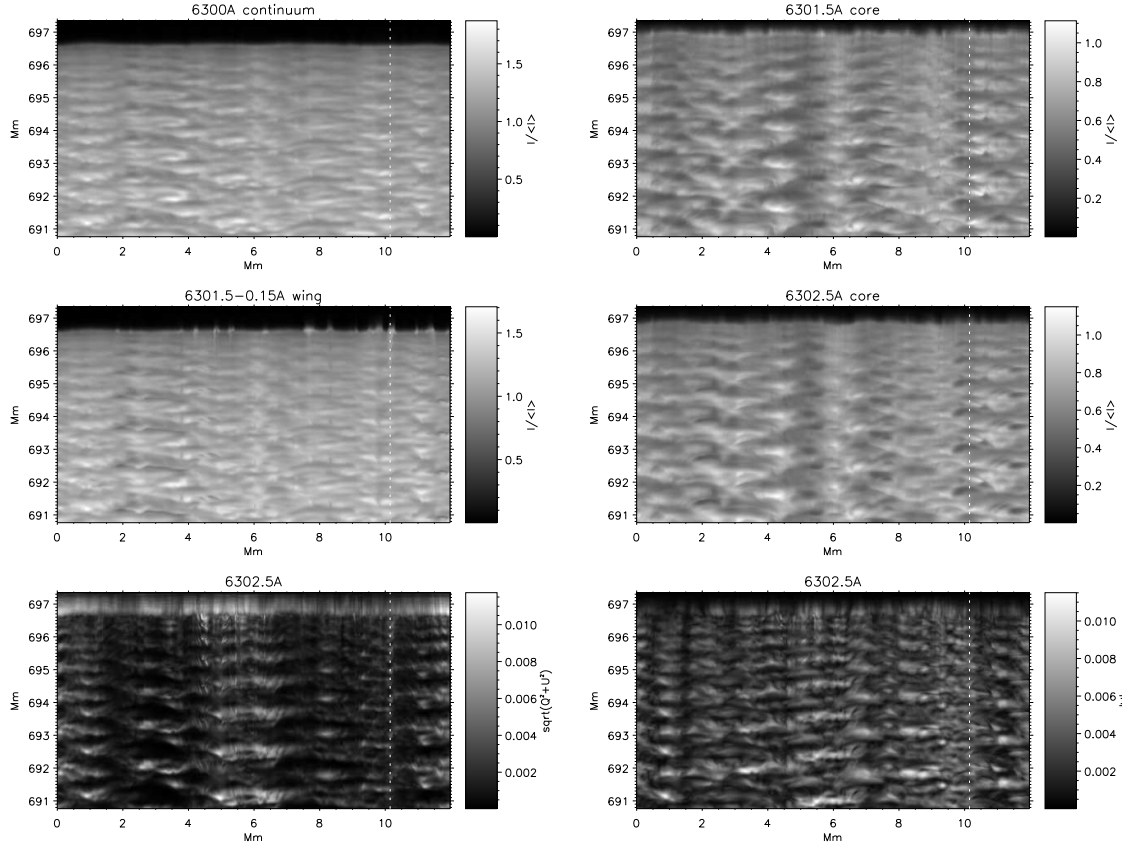


FIG. 4.— Continuum (top left), 6301.5Å line core (top right), 6301.5 – 0.15Å line wing (middle left), 6302.5Å (middle right) line core normalised intensity images from the simulations, and  $\int \sqrt{Q^2 + U^2} d\lambda$  (bottom left) and  $\int |V| d\lambda$  (bottom right) simulated images. Small-scale local brightenings are visible in 6301.5Å line wing, and, to some extent, in the line cores. Integrated Stokes parameters show presence of both circular and linear polarisation. The linear polarisation is significantly more pronounced above the simulated limb compared to the circularly polarized light in the same region.

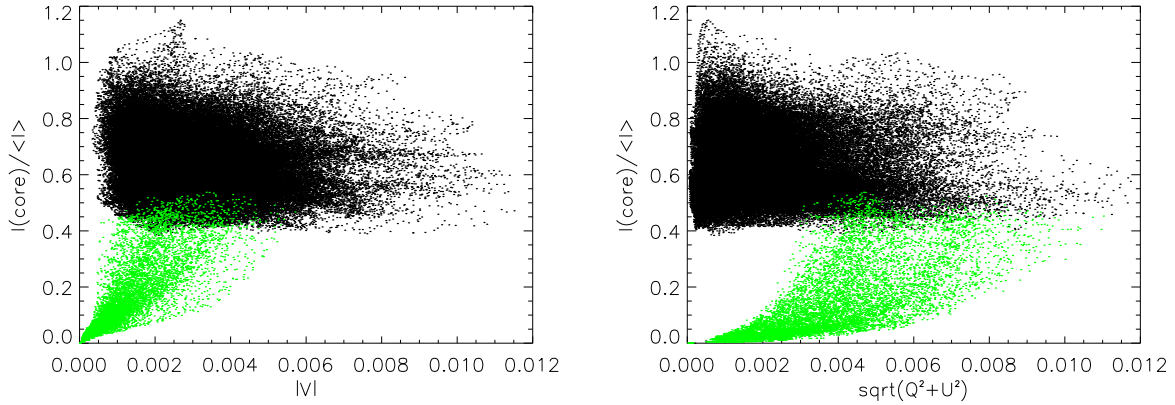


FIG. 5.— Scatter plots of intensity in the line core vs the total Stokes- $V$  area (left panel) and of intensity in the line core vs the total Stokes- $\sqrt{Q^2 + U^2}$  area (right panel) for FeI 6302.5Å line. The green dots correspond to the  $r > 696.8$  Mm in Fig. 4.

the solar limb (marked by green dots) and at the solar disk (black dots). While the solar disk population does not show a dependence of the FeI 6302.5Å line core intensity on the magnetic field, the solar limb population demonstrates such dependence: the larger the linear and/or circular polarisation, the higher the line core intensity is.

The horizontally averaged Stokes- $I$ ,  $Q/I$ ,  $U/I$ , and  $V/I$  profiles for 6301.5Å and 6302.5Å lines across the solar limb are shown in Fig. 6 for the radii  $R =$

695.875, 696.6, 696.675, 696.775, 697.2 Mm. The pure absorption profiles are obtained for the position within the simulated solar disk at  $R = 695.875$  Mm. Stokes- $Q$  and  $V$  show the presence of strong linear (vertical) and line-of-sight polarisation signals. At the limb,  $R = 696.6$  Mm, Stokes- $I$  profiles show an absorption core, while the profile wings show emission.

Stokes- $V$  profiles have lower amplitude compared to the disk due to the inclination of magnetic field with respect to the LOS, and the multi-lobed structure of

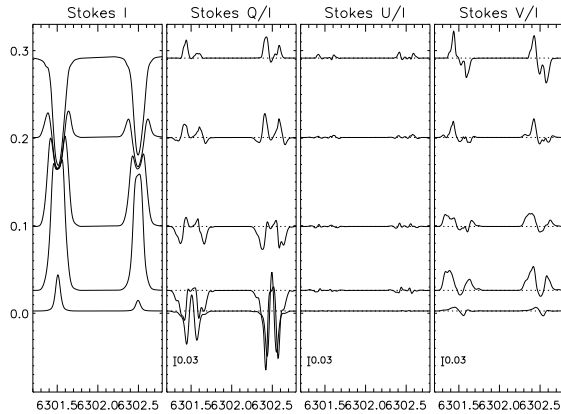


FIG. 6.— Horizontally averaged Stokes- $I$ ,  $Q/I$ ,  $U/I$ ,  $V/I$  profiles for the radii  $R = 695.875, 696.6, 696.675, 696.775, 697.2$  Mm (from the top to the bottom) in the model. The dotted lines show zero levels for  $Q/I$ ,  $U/I$  and  $V/I$  profiles, which are normalised so one tick interval in the corresponding plots is equal to 0.03.

the profiles becomes more pronounced due to presence of both positive and negative polarities of the magnetic field and velocity variations along the LOS and within the horizontal averaging element.

Above the limb, Stokes- $I$  become gradually more emissive in the optically thin part of the simulated atmosphere. In agreement with the observations (Lites et al. 2010), the 6302.5 Å line profile becomes entirely emissive closer to the limb than the 6301.5 Å profile. At about 300 km above the simulated limb both lines are in the emission regime. In the topmost layers of the simulation domain, both lines become fully emissive with no core absorption. The line intensity ratio of 3.4, which is close to the ratio of the values of the oscillator strengths used for the lines  $\sim 3.47$  (see Section 1) indicates optically thin emission regime of the lines. Stokes- $Q$  profiles demonstrate strong linear polarisation above the limb, while Stokes- $V$  becomes somewhat smaller, complex and multi-lobed, indicating that the LOS velocity and magnetic field experience significant changes in the region of the line formation. Stokes- $U$  does not show any significant horizontal polarisation due to the geometry of the magnetic field in the simulation.

Lites et al. (2010) suggested that the Fe I 6301.5 Å and 6302.5 Å line profile reversals to the emission regime in the wings in proximity to the solar limb are caused by non-LTE excitation of iron atoms by scattered light coming from the photosphere. Our simulation, however, shows the presence of such horizontally average profiles, computed using the pure one-dimensional LTE approximation. To determine the physical mechanism of the wing emission, we first performed the computation of the Fe I line profiles in the horizontally averaged model with zero LOS velocity. This simple numerical experiment showed the absence of emission wings in the computed line profiles and LTE-type transition of the lines from the absorption to emission regime across the simulated solar limb. Therefore, in the simulation we present here, the wing emission in the horizontally-averaged profiles is created by the superposition of the local, possibly asymmetric emission-absorption profiles produced by strong LOS (tangential to the solar surface) velocity and temperature gradients at the corrugated surface of the solar limb. In the next subsection, we analyse the details of

formation of these profiles in our simulations.

### 3.2. Absorption-emission profiles at the solar limb

Figure 7 shows simulated  $I$ ,  $Q/I$ ,  $U/I$  and  $V/I$  slit images for the horizontally-averaged simulated profiles (top row), for a slit positioned vertically across the solar limb at the position marked by the vertical dotted line in Fig. 4 (middle row), and for the slit positioned horizontally at the solar limb, as marked in the top-left (Stokes- $I$ ) panel of the figure (bottom row).

The horizontally-averaged Stokes- $I$  profiles show absorption within the simulated solar disk, the emission profiles far above the solar limb, and the transition from pure absorption to pure emission, which is characterised by the presence of the profiles with the absorption core and the raised, emissive wings. Stokes- $Q/I$  profiles within the disk are positive predominantly because the magneto-convection model used in this simulation has a unipolar vertical magnetic field. Above the limb, Stokes- $Q/I$  change their signs. Horizontally-averaged Stokes- $U/I$  profiles generally have multi-lobed shapes and lower amplitudes, as has already been shown, due to the absence of a preferred direction for the magnetic fields parallel to the limb in the simulation. Stokes- $V/I$  profiles, while also being complex and multi-lobed, show some preference towards positive blue lobes at the disk, which is consistent with the geometry of magnetic field in opening magnetic flux tubes of positive polarity.

For the vertically-aligned slit, the Stokes- $I$  slit image shows strong continuum variability on the disk and emission cores above the limb for both the lines. However, the most pronounced feature in the image is the presence of bright features in the blue wings<sup>1</sup> of both 6301.5 and 6302.5 Å Fe I lines with the intensities higher and spatially unrelated to the continuum intensity enhancements. At the same locations as the bright features in the Stokes- $I$  wings, Stokes- $Q/I$  and  $U/I$  show strong polarisation signals and rapidly change sign within the same intensity feature. Notably, Stokes- $Q/I$  and  $U/I$  are, in general, of similarly large amplitudes ( $\pm 0.4$ ), indicating the presence of strong perpendicular to the LOS magnetic fields. Above the limb, Stokes- $Q/I$  show a multi-lobed structure, which does not vary with height significantly, while Stokes- $U/I$  vanishes. Stokes- $V/I$  signals within the disk show multiple lobes of both polarities too, indicating the presence of the gradients of LOS velocity and magnetic fields (see e.g. Shelyag et al. 2007). It should be noted that no averaging or image degradation has been applied for the shown vertically-aligned slit, therefore the only source of strongly asymmetric multi-lobed Stokes- $V$  profiles is the variation of the physical parameters along the LOS.

Above the limb, Stokes- $V/I$  vanishes in agreement with the bottom-right panel of Fig. 4.

The Stokes- $I$ ,  $Q/I$ ,  $U/I$  and  $V/I$  images for the horizontally-positioned slit at the solar limb are shown in the bottom row of Fig. 7. The Stokes- $I$  image shows the presence of profiles with emission wings almost everywhere along the slit for both lines. It should be noted

<sup>1</sup> Note that the presence of only the blue wing emission here is purely a selection effect introduced by choosing a position with a bright feature in the blue wing of the profile. Similarly frequent features in the red wing are also found in the simulations, as well as the features with two emissive lobes of lower amplitude.

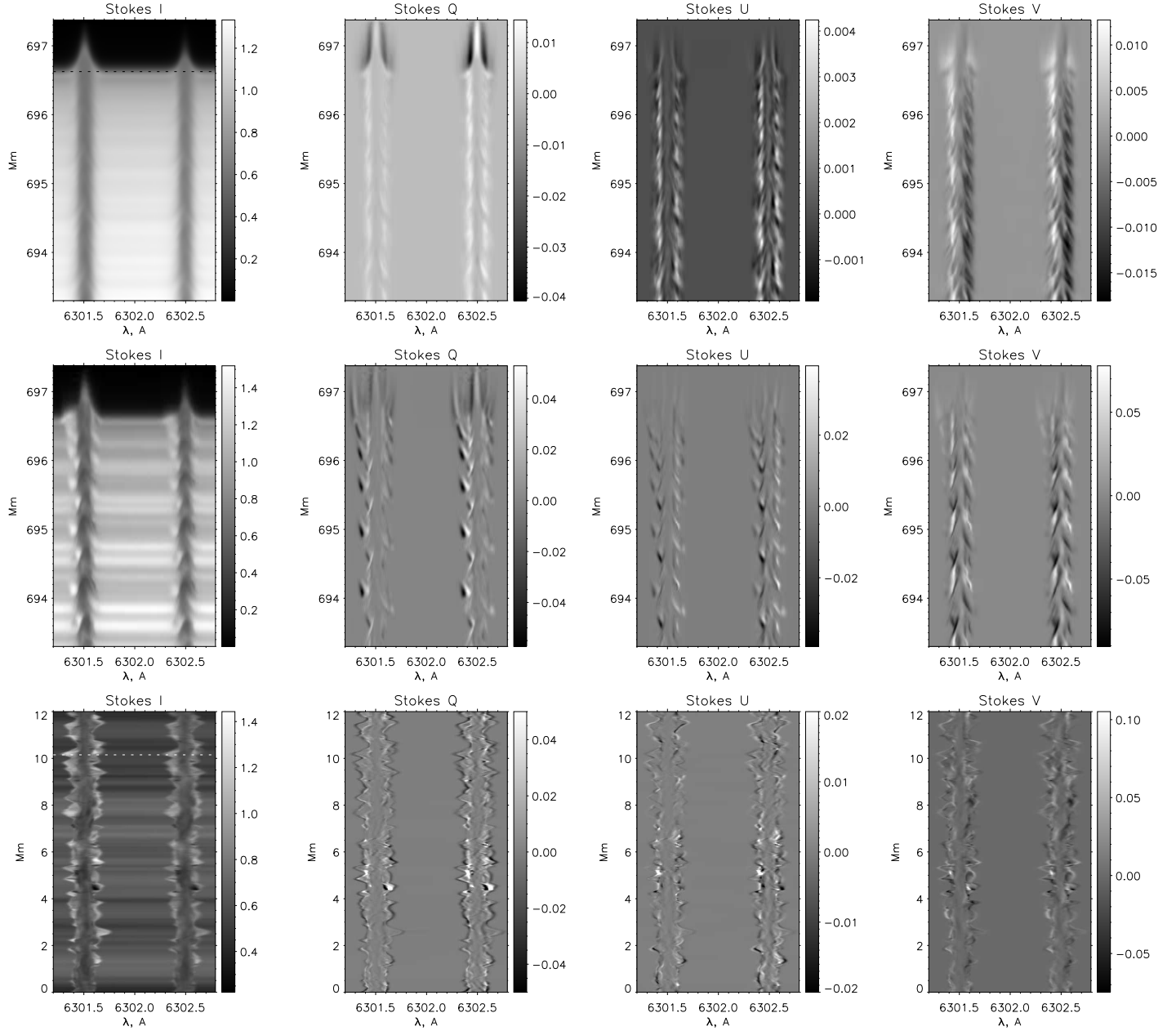


FIG. 7.— Simulated  $I$ ,  $Q/I$ ,  $U/I$ ,  $V/I$  slit images for the horizontally averaged profiles (top row), for a position across the simulated solar limb marked by the dotted line in Fig. 4 (middle row), and for a slit positioned horizontally at the limb (bottom row, marked in the top row Stokes- $I$  image with the dashed line). The position of the vertical slit shown in the middle row is marked by the horizontal dashed line in the bottom row.

that most of the profiles are strongly asymmetric, with emission either in the blue or in the red lobe. The presence of the emission lobes shows some correlation with the continuum intensity variation. The emission lobes are strongly shifted with the corresponding LOS velocities of  $4 - 8 \text{ km s}^{-1}$ . There is a weak visual correlation between Stokes- $Q/I$ ,  $U/I$  amplitudes and the emission lobes, while Stokes- $Q/I$  has expectedly larger amplitude than Stokes- $U/I$ . Nevertheless, the Stokes- $Q/I$  and  $U/I$  signal patterns coincide with the emission lobes of the profiles, while there are no strong signals in the line absorption cores. A similar dependence is found for the Stokes- $V/I$  signal.

The process of formation of the profiles which show

both emission and absorption is analysed below. An arbitrary position within the simulated solar disk, but close to the limb was selected, where the 6301Å line profile shows both absorption in the line core and emission in the blue wing. Response functions (RFs) of all Stokes parameters to a small temperature perturbation ( $\Delta T = 100 \text{ K}$ ) in the corresponding one-dimensional atmosphere were computed. Fig. 8 shows the calculated RFs (grayscale images) together with the corresponding line profiles (plots in the top row), and the photospheric parameters (vertical plots). A clear correspondence is seen between the emission part of the profile at  $\Delta\lambda = -0.1\text{Å}$ , and a sharp temperature rise at about 1.5 Mm distance along the LOS. At the same location,

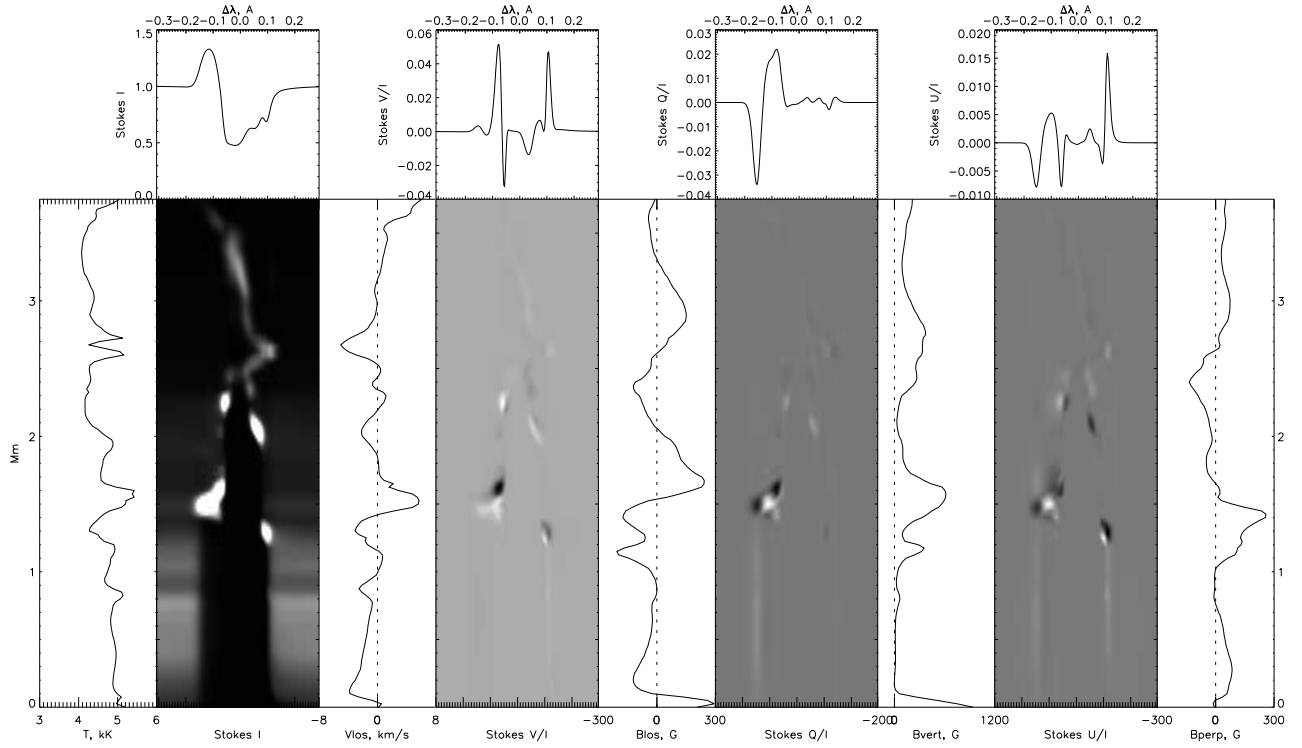


FIG. 8.— Simulated  $I$ ,  $Q/I$ ,  $U/I$ ,  $V/I$  profiles (top row), their response functions to the temperature perturbation (grayscale images) and the structure of the corresponding 1D atmosphere along the LOS. Dashed vertical lines mark zero values for  $v_{los}$ ,  $B_{los}$ ,  $B_{||}$  and  $B_{\perp}$ .

a strong plasma flow of about  $4 - 5 \text{ km s}^{-1}$  towards the observer is found, which shifts the emission wavelength towards the blue side of the spectrum. The LOS component of the magnetic field  $B_{los}$  changes the direction and amplitude from  $-200 \text{ G}$  to  $250 \text{ G}$ , leading to the formation of a strong and asymmetric Stokes- $V/I$  signal at the same wavelength (see e.g. Shelyag et al. 2007). The vertical, perpendicular to the LOS component of the magnetic field  $B_{||}$  is almost always positive with the minimum magnetic field of a few Gauss. In the emission region it increases up to about  $600 \text{ G}$ , indicating that the line-of-sight crosses an intergranular magnetic field concentration there. The Stokes- $U/I$  RF has a maximum in this region, and the Stokes- $U/I$  profile shows two lobes of large amplitude in the blue. The horizontal, perpendicular to the LOS magnetic field component  $B_{\perp}$  has expectedly smaller amplitude and also shows an increase in the emission region up to  $250 \text{ G}$ .

A summary of the process of photospheric emission-absorption Fe I line profile formation is provided in Fig. 9. The line-of-sight crosses three distinct regions. The first region (A) is above the granule, where both the LOS components of the velocity and the magnetic field are small (from 0 to about  $1.0 \text{ Mm}$  along the LOS in Fig. 8). In this region, the continuum radiation is formed. Then, the line-of-sight crosses the intergranular magnetic field concentration region (B). Strong torsional oscillatory motions with speeds of a few  $\text{km s}^{-1}$  within the magnetic concentration (Shelyag et al. 2013; Shelyag & Przybylski 2014) Doppler-shift the line formation wavelength in accordance to the direction of motion in this region (from

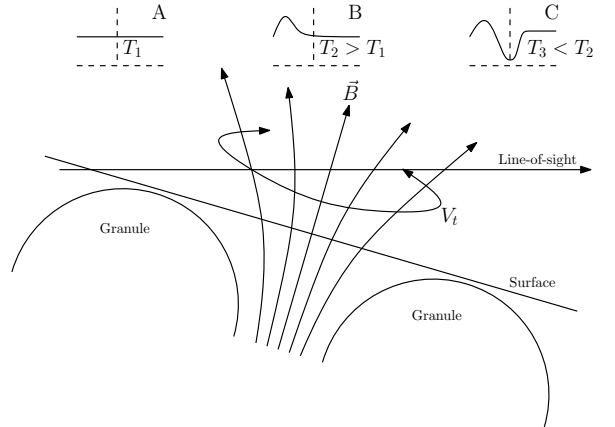


FIG. 9.— Emission-absorption line profile formation in the non-uniform solar photosphere at the limb. The line-of-sight close to the solar limb crosses three different regions: (A) a non-magnetic granular region, where the continuum radiation is formed, (B) the intergranular magnetic field concentration, where the emission part of the profile is formed, and which is characterised by radiative heating, positive temperature gradient ( $T_2 > T_1$ ), and torsional plasma motions ( $V_t$ ), and (C) a non-magnetic region over the granule with a negative temperature gradient ( $T_3 < T_2$ ), where the absorption part of the profile is formed.

$1.0$  to  $2.0 \text{ Mm}$  in Fig. 8). At the same time, radiative heat exchange with the hot granular wall (see e.g. Spruit 1976; Vögler et al. 2004) and resistive heating



(Moll et al. 2012; Shelyag & Przybylski 2014) cause the localised temperature increase within the magnetic flux tube and emission. Finally, the line-of-sight leaves the magnetic field concentration and enters the rarified region above the next granule (C), where the LOS velocities are generally smaller and temperature decreases (up to the chromospheric layers, to which the photospheric lines under consideration are not sensitive), leading to the formation of an absorption line core.

#### 4. DISCUSSION

In this paper, we presented a novel spectropolarimetric simulation of photospheric radiation at the solar limb. We used a single snapshot from magnetoconvection simulations of a plage region to construct a cylindrical solar limb-like region and performed detailed radiative diagnostics computation on this domain with the 6301.5Å and 6302.5Å pair of photospheric lines of neutral iron in the LTE approximation. We computed the average radiation parameters at the transition between the solar disk and limb, such as limb darkening, *rms* granulation contrast and average Stokes profiles.

The average Stokes profiles showed the emission above the limb, the presence of emissive line wings, absorption core and significant polarisation signal at the limb, similar to the observations (Lites et al. 2010), where it was suggested that the emissive wings are the result of radiation scattering and non-LTE excitation in the solar atmosphere. Our results, however, suggest that the radiation scattering at the limb is not the only mechanism causing the emission in the line wings. It is demonstrated that, in the LTE approximation, the emission lobes in Stokes-*I* profiles at the limb can be formed due to the presence of the torsional bidirectional flows along the line-of-sight and the local heating in the intergranular magnetic field concentrations. When the line-of-sight, along which the radiation is formed, crosses the intergranular magnetic concentration region, it experiences a temperature rise, leading to emission, and a Doppler shift to the blue (or red) side of the spectrum. After that, the line-of-sight crosses an absorption region with a smaller LOS velocity and a temperature decrease, which leads to the formation of the absorption core. As there is no preferred direction for the torsional flows in magnetic field concentrations, both blue- and red-wing emission is observed in the simulations. The profiles with two emissive lobes are also found in the regions where the line-of-sight crosses the layers of opposite rotation in the magnetic flux tubes (Shelyag et al. 2011b). When averaged spatially, these profiles lead to the appearance of the Stokes-*I* profiles with emissive lobes and absorption core. The polarisation signals at the limb show the presence of vertically (radially) oriented magnetic fields, which is expected since a plage model with 200 G vertical magnetic field was used for the computation.

Despite the detailed characteristics of torsional motions in magnetic field concentrations still need to be

better understood (see e.g. Wedemeyer & Steiner 2014), there is little doubt of their presence in the magnetic field concentrations. Furthermore, non-magnetic or weakly magnetised photospheric models also show torsional motions in intergranular lanes (Shelyag et al. 2011a; Moll et al. 2011; Kitiashvili et al. 2012, 2013). While in this case of zero or weak photospheric magnetic field the magnetic tension is small and does not prevent tornado-like appearance of the vortex, the purely hydrodynamic vortex flows in the intergranular lanes would lead to the presence of torsional motions consequently leading to the similar mechanism of emission-absorption line profile formation at the solar limb.

A natural point of concern is the use of LTE approximation in the presented study. While there is no doubt the non-LTE effects are important especially at the limb, the primary aim of the study was to demonstrate the LTE effects of the limb radiation formation. Furthermore, the neutral iron lines used for spectropolarimetric diagnostics in this paper are formed low in the photosphere irrespectively of the position at the solar disk, where the LTE assumption is still reasonable, at least for the intergranular lanes (Shchukina & Trujillo Bueno 2001). The basic process of emission-absorption line profiles formation at the limb, which is described in the paper, relies on the presence of torsional motions and heating within the intergranular magnetic flux tubes.

The structures described in the paper are rather small-scale, with linear dimensions of about 100 km. Taking into account low light and high noise levels, inevitably associated with limb observations, it would be difficult to provide detailed and direct observational confirmation of the effect of torsional flows in magnetic field concentrations on the photospheric line formation at the solar limb. Nevertheless, future, large-scale instruments, such as DKIST, will be able to observe these small features. Finally, further study is needed and planned to analyse their lifetimes and links to chromospheric fine structure, bidirectional flows and oscillations (Sekse et al. 2013).

#### 5. ACKNOWLEDGEMENT

The author thanks the anonymous referee for his valuable comments. This research was undertaken with the assistance of resources provided at the NCI National Facility systems at the Australian National University through the National Computational Merit Allocation Scheme supported by the Australian Government, and at the Multi-modal Australian ScienceS Imaging and Visualisation Environment (MASSIVE) ([www.massive.org.au](http://www.massive.org.au)). The author also thanks Centre for Astrophysics & Supercomputing of Swinburne University of Technology (Australia) for the computational resources provided. Dr Shelyag is the recipient of an Australian Research Council's Future Fellowship (project number FT120100057).

#### REFERENCES

- Beeck, B., Collet, R., Steffen, M., et al. 2012, *A&A*, 539, A121  
 Cheung, M. C. M., Schüssler, M., & Moreno-Insertis, F. 2007, *A&A*, 461, 1163  
 Irwin, A. W. 2012, *Astrophysics Source Code Library*, 11002  
 Keller, C. U., Schüssler, M., Vögler, A., & Zakharov, V. 2004, *ApJ*, 607, L59  
 Kitiashvili, I. N., Kosovichev, A. G., Mansour, N. N., Lele, S. K., & Wray, A. A. 2012, *Phys. Scr*, 86, 018403

- Kitiashvili, I. N., Kosovichev, A. G., Lele, S. K., Mansour, N. N., & Wray, A. A. 2013, *ApJ*, 770, 37
- Kitiashvili, I. N., Couvidat, S., & Lagg, A. 2014, arXiv:1407.2663
- Koesterke, L., Allende Prieto, C., & Lambert, D. L. 2008, *ApJ*, 680, 764
- Leenaarts, J., Carlsson, M., & Rouppe van der Voort, L. 2012, *ApJ*, 749, 136
- Lites, B. W., Casini, R., Manso Sainz, R., et al. 2010, *ApJ*, 713, 450
- Moll, R., Cameron, R. H., & Schüssler, M. 2011, *A&A*, 533, A126
- Moll, R., Cameron, R. H., & Schüssler, M. 2012, *A&A*, 541, A68
- Sekse, D. H., Rouppe van der Voort, L., De Pontieu, B., & Scullion, E. 2013, *ApJ*, 769, 44
- Pereira, T. M. D., Asplund, M., Collet, R., et al. 2013, *A&A*, 554, A118
- Shchukina, N., & Trujillo Bueno, J. 2001, *ApJ*, 550, 970
- Shelyag, S., Schüssler, M., Solanki, S. K., Vögler, A. 2007, *A&A*, 469, 731
- Shelyag, S., Keys, P., Mathioudakis, M., & Keenan, F. P. 2011, *A&A*, 526, A5
- Shelyag, S., Fedun, V., Keenan, F. P., Erdélyi, R., & Mathioudakis, M. 2011, *Annales Geophysicae*, 29, 883
- Shelyag, S., Cally, P. S., Reid, A., & Mathioudakis, M. 2013, *ApJ*, 776, L4
- Shelyag, S., & Przybylski, D. 2014, arXiv:1405.5954
- Socas-Navarro, H., Trujillo Bueno, J., & Ruiz Cobo, B. 2000, *ApJ*, 544, 1141
- Socas-Navarro, H. 2011, *A&A*, 529, A37
- Socas-Navarro, H., de la Cruz Rodriguez, J., Asensio Ramos, A., Trujillo Bueno, J., & Ruiz Cobo, B. 2014, arXiv:1408.6101
- Spruit, H. C. 1976, *Sol. Phys.*, 50, 269
- Stein, R. F. 2012, *Living Reviews in Solar Physics*, 9, 4
- Tsuneta, S., Ichimoto, K., Katsukawa, Y., et al. 2008, *Sol. Phys.*, 249, 167
- Vögler, A., Bruls, J. H. M. J., & Schüssler, M. 2004, *A&A*, 421, 741
- Vögler, A., Shelyag, S., Schüssler, M., Cattaneo, F., Emonet, T., & Linde, T. 2005, *A&A*, 429, 335
- Wedemeyer, S., & Steiner, O. 2014, arXiv:1406.7270